

Adsorption of $[\text{AuCl}_4]^-$ on Ultrasonically and Mechanical-Stirring Assisted Mg/Al- NO_3 Hydrotalcite-Magnetite

Triastuti Sulistyaningsih^{1,2,*}, Sri Juari Santosa², Dwi Siswanta², and Bambang Rusdiarso²

¹Department of Chemistry, Semarang State University, Sekaran, Gunungpati Semarang, Central Java 50229, Indonesia

²Department of Chemistry, Faculty of Mathematics and Natural Sciences, Universitas Gadjah Mada Sekip Utara PO BOX BLS 21 Yogyakarta 55281, Indonesia

Received December 7, 2015; Accepted April 26, 2016

ABSTRACT

It has been examined the application of Mg/Al- NO_3 hydrotalcite-magnetite synthesized mechanically (MHT) and ultrasonically (UMHT) by co-precipitation method as adsorbents for $[\text{AuCl}_4]^-$ from aqueous solution. Two techniques of synthesis were conducted to determine the effect on the increase of adsorption ability of the $[\text{AuCl}_4]^-$. Magnetite and Mg/Al- NO_3 hydrotalcite-magnetite synthesized by co-precipitation with modifications hydrothermal treatment at 120 °C for 5 h. The adsorbents were characterized by Fourier Transform Infrared (FTIR) spectroscopy, X-ray diffraction (XRD), Scanning electron microscopy (SEM), Brunauer-Emmett-Teller (BET) and Vibrating sample magnetometer (VSM). Adsorption studies were done by getting the optimum pH, optimum contact time and the optimum concentration. A result of the adsorption study of $[\text{AuCl}_4]^-$ on both adsorbents was optimum at pH 3 and fitted well to Langmuir isotherm and pseudo second-order kinetic models. The adsorption capacity of UMHT (ultrasonic technique) was 66.67 mg g^{-1} and it was higher than that of MHT (mechanic technique), i.e. 31.25 mg g^{-1} . This shows that the ultrasonic radiation technique can increase the adsorption capacity of the $[\text{AuCl}_4]^-$. Based on the desorption using 0.5 mol L^{-1} NaOH solution, more $[\text{AuCl}_4]^-$ was eluted from MHT, indicating that $[\text{AuCl}_4]^-$ was weakly bound on MHT than UMHT.

Keywords: $[\text{AuCl}_4]^-$; magnetite; hydrotalcite; ultrasonic assisted; adsorption

ABSTRAK

Telah diuji aplikasi Mg/Al- NO_3 hidrotalsit-magnetit yang disintesis secara mekanik dan ultrasonik dengan metode ko-presipitasi sebagai adsorben $[\text{AuCl}_4]^-$ dalam larutan. Dua teknik sintesis digunakan untuk mengetahui efek pada peningkatan kemampuan adsorpsi terhadap $[\text{AuCl}_4]^-$. Magnetit dan Mg/Al- NO_3 hidrotalsit-magnetit disintesis secara ko-presipitasi dengan modifikasi perlakuan hidrotermal pada suhu 120 °C selama 5 jam. Adsorben dikarakterisasi menggunakan by Fourier Transform Infrared (FTIR) spectroscopy, X-ray diffraction (XRD), Scanning electron microscopy (SEM), Brunauer-Emmett-Teller (BET) dan Vibrating sample magnetometer (VSM). Kajian adsorpsi dilakukan untuk mendapatkan pH optimum, waktu kontak optimum dan konsentrasi optimum. Hasil kajian adsorpsi $[\text{AuCl}_4]^-$ pada kedua adsorben menunjukkan optimum adsorpsi terjadi pada pH 3 dan sesuai dengan isotherm Langmuir serta model kinetika orde dua semu. Kapasitas adsorpsi UMHT (teknik ultrasonik) terhadap $[\text{AuCl}_4]^-$ adalah 66,67 mg g^{-1} dan lebih tinggi daripada MHT (teknik mekanik), yaitu 31,25 mg g^{-1} . Hal ini menunjukkan bahwa teknik radiasi ultrasonik dapat meningkatkan kapasitas adsorpsi $[\text{AuCl}_4]^-$. Berdasarkan kajian desorpsi menggunakan larutan NaOH 0,5 mol L^{-1} , $[\text{AuCl}_4]^-$ yang terelusi dari MHT lebih banyak, menunjukkan bahwa $[\text{AuCl}_4]^-$ terikat lebih lemah pada MHT daripada UMHT.

Kata Kunci: $[\text{AuCl}_4]^-$; magnetit; hidrotalsit; ultrasonik; adsorpsi

INTRODUCTION

The growing amount of electrical and electronic waste (e-waste) is creating negative impacts on the environment and also bringing serious problems with regard to the supply of raw materials, especially precious metals which are not only scarce but also very essential

for these advanced devices [1]. In some cases, the precious metal contents of the wastes disposed of in this form are unexpectedly higher than that in the ore itself [2]. Economically, gold has been historically important as currency and remain important as an investment commodity. Considering its value and scarcity, it is important to treat the aqueous waste

* Corresponding author. Tel : +62-8156589843
Email address : triastuti.s@gmail.com

solution and try to recover gold economically. Nevertheless, the separation and recovery of gold is not actually simple, which is due to the low concentration of gold in environmental, geological and metallurgical materials and insufficient sensitivity [3]. Various technologies that have been employed for the recovery and enrich gold include co-precipitation [4], ion exchange [5-6], solvent extraction [7] and adsorption [3,8-9].

Hydrotalcite (HT) as an anionic clay is generally expressed as $[M_{1-x}^{2+}M_x^{3+}(\text{OH})_2]^{x+}(\text{A}^{n-})_{x/n} \cdot m\text{H}_2\text{O}$, where M^{2+} represents divalent metal cation (Ca^{2+} , Mg^{2+} , Zn^{2+} , Ni^{2+} , Fe^{2+} , or Mn^{2+}), M^{3+} is trivalent metal cation (Al^{3+} , Cr^{3+} , Mn^{3+} , Fe^{3+} or Ni^{3+}) and A^{n-} is an anion (CO_3^{2-} , NO_3^- , SO_4^{2-} , or Cl^-). x is denotes as the molar ratio of M^{3+} to total metal, ranging from 0.15 to 0.33 for pure HT formation [10]. HT has exhibited its promising application in the adsorption of $[\text{AuCl}_4]^-$ due to its high surface area and anion exchange property. Despite, it is still an issue that the separation of HT from water is difficult in the industrial applications, especially in the treatment of river, lake and other natural water.

On the other hand, magnetic separation is a very convenient approach for removing and recycling magnetic particles/composite [11]. For this aim, magnetic material like Fe_3O_4 is prepared and widely used due to its unique magnetic response and large surface area [8,12]. The magnetite (Fe_3O_4) can be modified with inorganic compounds to obtain magnetic adsorbents. Accordingly, the combination of magnetic compound and HT has been developed recently to enhance separation and re-dispersion performance of HT in aqueous solution [13-14].

In this study, we prepare and characterize a magnetic Mg/Al- NO_3 HT-magnetite by mechanically and sonochemically assisted co-precipitation methods and investigate adsorption performance that adsorbent for $[\text{AuCl}_4]^-$. The ultrasonic radiation assistance can shorten the preparation time and decreased the size of the composite particles and be favorable to increase the adsorption capacity. Desorption process also has been done using NaOH solution to investigate the possibility of Mg/Al- NO_3 hydrotalcite-magnetite to be regenerated.

EXPERIMENTAL SECTION

Materials

Analytical grade $\text{FeSO}_4 \cdot 7\text{H}_2\text{O}$, $\text{FeCl}_3 \cdot 6\text{H}_2\text{O}$, $\text{Mg}(\text{NO}_3)_2 \cdot 6\text{H}_2\text{O}$, $\text{Al}(\text{NO}_3)_3 \cdot 9\text{H}_2\text{O}$, $\text{NH}_3 \cdot \text{H}_2\text{O}$ (25%, w/w), NaOH, and HCl were purchased from Merck (Germany). Carbonate-free distilled water was used for a preparation of the solution and for rinsing the product.

Instrumentation

Characterization of magnetite and Mg/Al- NO_3 HT-magnetite before and after adsorption was performed using a Shimadzu FTIR-820 IPC for the functional group identification and a Shimadzu XRD-6000 for the crystallinity. The magnetic properties of the as-synthesized nanopowder were analyzed by Vibrating sample magnetometer (VSM) type OXFORD VSM 1.2H. The morphology of samples was viewed by Scanning electron microscopy (SEM) of a JSM-6360 instrument. Brunauer-Emmett-Teller (BET) surface area was determined by nitrogen adsorption/desorption using Gas Sorption Analyzer. The concentrations of $[\text{AuCl}_4]^-$ in the adsorption experiment were analyzed using Atomic Absorption Spectroscopy (AAS, Analytic Jena ContraAA 300, $\lambda = 242.8 \text{ nm}$).

Procedure

Synthesis of magnetite, Fe_3O_4

Fe_3O_4 were synthesized by an ultrasonic-assisted and under mechanical stirring co-precipitation method. In a typical procedure for an ultrasonic assisted, $\text{FeSO}_4 \cdot 7\text{H}_2\text{O}$ (6.95 g) and $\text{FeCl}_3 \cdot 6\text{H}_2\text{O}$ (10.12 g) were dissolved in 25 mL distilled water. An NH_4OH (3.5 M) solution was added dropwise into the mixed $\text{Fe}^{2+}/\text{Fe}^{3+}$ solution at 50 °C under ultrasonic irradiation, which was carried out in an ultrasound clean bath operating at 47 kHz with a power of 130 W (B 3210E-MT EMA-9408, USA) to increase pH until 11 for 1 h. After 1 h aging, the products were separated, washed with distilled water to neutral pH and then dried to obtain magnetite ultrasonic-assisted (UM). For synthesis under mechanical stirring (MM), the procedure was similar to the ultrasonic-assisted technique, but without the use of ultrasonic clean bath and the reaction was prolonged to 3 h.

Synthesized of Mg/Al- NO_3 hydrotalcite-magnetite

Mg/Al- NO_3 HT-magnetite were also synthesized by an ultrasonic-assisted and under mechanical stirring co-precipitation method. Procedure for the ultrasonic-assisted technique, the Fe_3O_4 powder (UM) (0.65 g) was redispersed in distilled water (50 mL). $\text{Mg}(\text{NO}_3)_2 \cdot 6\text{H}_2\text{O}$ (12.80 g, 0.05 mol) and $\text{Al}(\text{NO}_3)_3 \cdot 9\text{H}_2\text{O}$ (9.40 g, 0.025 mol) with the $\text{Mg}^{2+}/\text{Al}^{3+}$ molar ratio of 2.0 was dissolved in distilled water (100 mL), and NaOH (6.60 g, 0.165 mol) was dissolved in distilled water (100 mL). The two solutions were added dropwise to the Fe_3O_4 dispersion at 55 °C for 1 h under atmospheric nitrogen under ultrasound irradiation. After 2 h for aging, the products was heated hydrothermally at 120 °C for 5 h and then separated, washed with distilled water, and then dried to obtain Mg/Al- NO_3 -HT

magnetite (UMHT). For synthesis under mechanical stirring technique (MHT), the procedure was similar to the above mentioned procedure except prolonging the aging time to 12 h and removing the ultrasonic irradiation.

Characterization of materials

The magnetite and Mg/Al-NO₃ HT-magnetite were first characterized for the functional groups using a Shimadzu FTIR-820 IPC in the transmission mode in spectroscopic grade KBr pellets for all the powders. XRD patterns of samples to study the crystalline structure were recorded using a Shimadzu XRD-6000 diffractometer with Ni-filtered Cu K α radiation ($\lambda = 0.15406$ nm) at voltage 40 kV and current 30 mA. The sample was scanned in steps of 0.02° (2θ) in the range from 0 to 70° with a count time of 4 s per step. The magnetic properties of the synthesized nanopowder were analyzed by VSM type OXFORD VSM 1.2 H. The morphology of samples was viewed by scanning electron microscopy (SEM) using a JSM-6360 instrument and elemental analysis using Atomic absorption spectroscopy (AAS).

Stability test of magnetite in Mg/Al-NO₃ hydrotalcite-magnetite

Ten milligrams of Mg/Al-NO₃ hydrotalcite-magnetite (MHT or UMHT) was added to a series of 10 mL of decarbonated distilled water and the acidity was adjusted to pH 2.5, 3, 4, 5, 6, 7, and 8 using NaOH or HCl solution. After the mixture was shaken for 90 min, the supernatant was separated from the solid using external magnet and then the supernatant was analyzed its concentration of Fe using AAS.

Adsorption studies

Study of medium acidity effect was carried out by a batch adsorption technique. A series of [AuCl₄]⁻ solution (10 mL, 25 ppm) were adjusted to pH 2, 3, 4, 5, 6, 7, and 8 by adding either HCl or NaOH solution. Into every [AuCl₄]⁻ solution, 10 mg of MHT (or UMHT) was poured and then shaken for 90 min. After that adsorbent particles were separated by external magnet. The concentrations of [AuCl₄]⁻ in the filtrate were analyzed using AAS.

Adsorption kinetic experiments of were carried out in a batch adsorption with prepared a series of [AuCl₄]⁻ solution (10 mL, 25 ppm) at optimum pH. Into every [AuCl₄]⁻ solution, 10 mg of MHT (or UMHT) was poured and then shaken for selected time periods. In each selected time period, the concentration of [AuCl₄]⁻ in the filtrate after separated with external magnet was analyzed using AAS.

Adsorption isotherm studies were conducted by prepared a series of 10 mL [AuCl₄]⁻ solution with various

concentration at optimum pH. Into every [AuCl₄]⁻ solution, 10 mg of MHT (or UMHT) was poured and then shaken for optimum contact time. After separated by external magnet, concentrations of [AuCl₄]⁻ in the filtrate were analyzed using AAS.

Desorption studies

In order to estimate the reversibility of [AuCl₄]⁻ sorption, desorption experiments using NaOH eluent have been carried out. NaOH solution with various concentrations was poured into MHT or UMHT that has been used for adsorption process and the mixtures were shaken for various time contacts. After separated by an external magnet, concentrations of [AuCl₄]⁻ in the filtrates were analyzed using AAS.

RESULT AND DISCUSSION

Characterization

FTIR characterization results for the synthesized magnetite with ultrasonic (UM) and with mechanical stirring technique (MM) yield clear absorption bands at a wavelength of 586 and 339; 354 cm⁻¹ which correspond to a strain of Fe-O tetrahedral and Fe-O octahedral of Fe₃O₄ (Fig. 1A). In addition, there are weak absorption bands at wavenumber 1627 and 3402 or 3448 cm⁻¹ which are the stretching vibration of OH groups on the surface of the magnetite indicating that the complete crystallization process [15-16]. The hydrolyzation on the surface of a Fe₃O₄ cause the presence of -OH groups shows the formation Fe(OH)₂, Fe(OH)₃ and FeOOH [17].

For the spectra of the UMHT and MHT before adsorption, they show a strong absorption band at wavenumber 1381 cm⁻¹ which is the NO₃ stretching vibration indicating that the nitrate anion presents on the interlayer of both UMHT and MHT [18]. Additionally, a weak absorption at wavenumbers 1635 cm⁻¹ shows the -OH vibrations of H₂O on the interlayer, and broader the absorption band at region wavenumber 3400 cm⁻¹ shows the -OH stretching vibration of Mg-OH and Al-OH [19-20]. A strong absorption at 655 cm⁻¹ (UMHT) and 648 cm⁻¹ (MHT) may be related to Me-O vibration such as Al-O, Mg-O and Fe-O. After adsorption, spectra of the UMHT and MHT yield absorption band at wavenumber which almost the same as wavenumber before adsorption. But, an area of the absorption band at region wavenumber 3400 and 600 cm⁻¹ after adsorption wider than before adsorption. This was caused by hydrogen bonding between the surfaces of Mg/Al-NO₃-HT with [AuCl₄]⁻.

The crystalline structures of magnetite and Mg/Al-NO₃-HT magnetite were shown in Fig. 1B. There are a

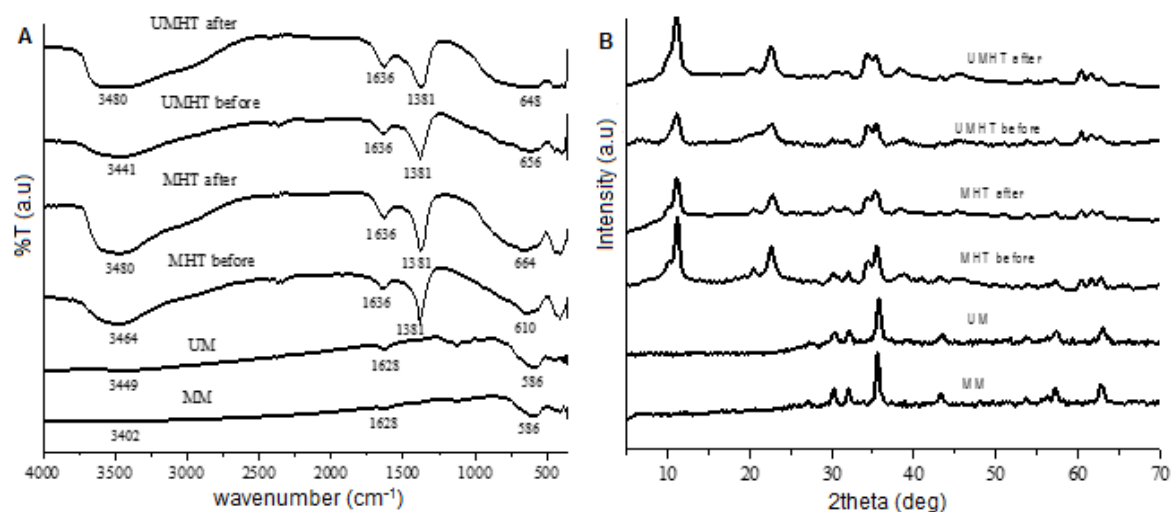


Fig 1. FTIR spectra (A) and XRD patterns (B) of the magnetites and Mg/Al-NO₃-HT magnetite before and after [AuCl₄]⁻ adsorption

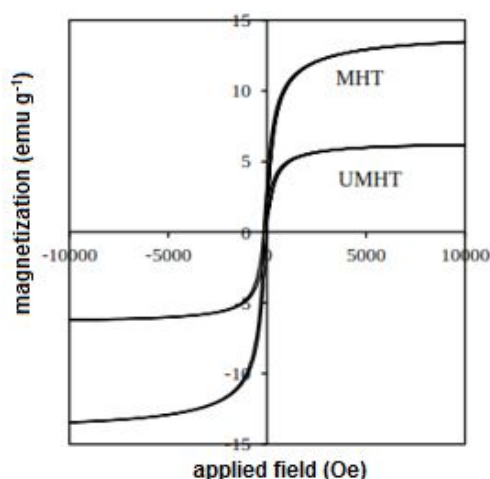


Fig 2. Magnetization curve of MHT and UMHT

series of characteristic peaks at $2\theta = 30.27^\circ$; 35.68° ; 43.30° ; 57.21° ; 62.90° ; and 74.51° which is the reflection (220), (311), (400), (511), (440) and (533) planes. They correspond to the standard data for Fe₃O₄ (JCPDS no. 89.0691). The XRD patterns of both the mechanically and ultrasonically prepared MHT are characteristic of hydrotalcite. The peak of MHT which corresponds to the reflection (009) is divided into two sub-peaks which the first one at a smaller diffraction angle shows the peak for Mg/Al-NO₃ hydrotalcite, whereas the second one at a slightly greater diffraction angle comes from the Fe₃O₄ particle core, on the surface of which the Mg/Al-NO₃ hydrotalcite is deposited [21]. Compared with the mechanically prepared sample with aging time 12 h, the ultrasonic assistance with an aging time of only 2 h produced intensity and sharpness of peak almost the same, indicating that the application of ultrasound clean bath in the preparation process promotes the formation

of the hydrotalcite-like phase. After adsorption, 2θ of the characteristic peak of Mg/Al-NO₃-HT magnetite is not significantly different. There is no increasing of d_{003} spacing which indicating that [AuCl₄]⁻ anion is not entering Mg/Al-NO₃-HT magnetite interlayer. Probably, [AuCl₄]⁻ anion was bound with a surface of Mg/Al-NO₃-HT protonated (Mg-OH₂⁺ or Al-OH₂⁺) through hydrogen bonding.

Magnetic properties were measured at room temperature using a VSM (Fig. 2). The results of measurements of the specific saturation magnetization (M_s) of the two samples of Mg/Al-NO₃ hydrotalcite, MHT and UMHT, yielded the value M_s of MHT (13.48 emu/g) that was higher than that of UMHT (6.18 emu/g). The M_s values decrease with decreasing particle size due to the reduction in crystallinity of the magnetic domain [15]. These results indicate that particle size of UMHT smaller than MHT. The SEM micrographs of magnetite (Fig. 3A and 3B) illustrate that the morphology of magnetite is spherical agglomerated with homogeneous size distribution. The magnetite which was synthesized sonochemically (UM = 14.6 nm) showed smaller particle size than mechanically synthesized magnetite (MM = 15.6 nm). It is proved that the sonochemical technique can reduce the size of the magnetite particles. For MHT and UMHT (Fig. 3C and 3D), it can be seen that in MHT, the MM particle is covering the surface of HT while in UMHT they may be agglomerated in HT due to relatively smooth surface of UMHT.

Effect of pH on [AuCl₄]⁻ Adsorption

Before being applied as adsorbents, the stability of magnetite on both MHT and UMHT was first determined. Stability of magnetite as measured as the

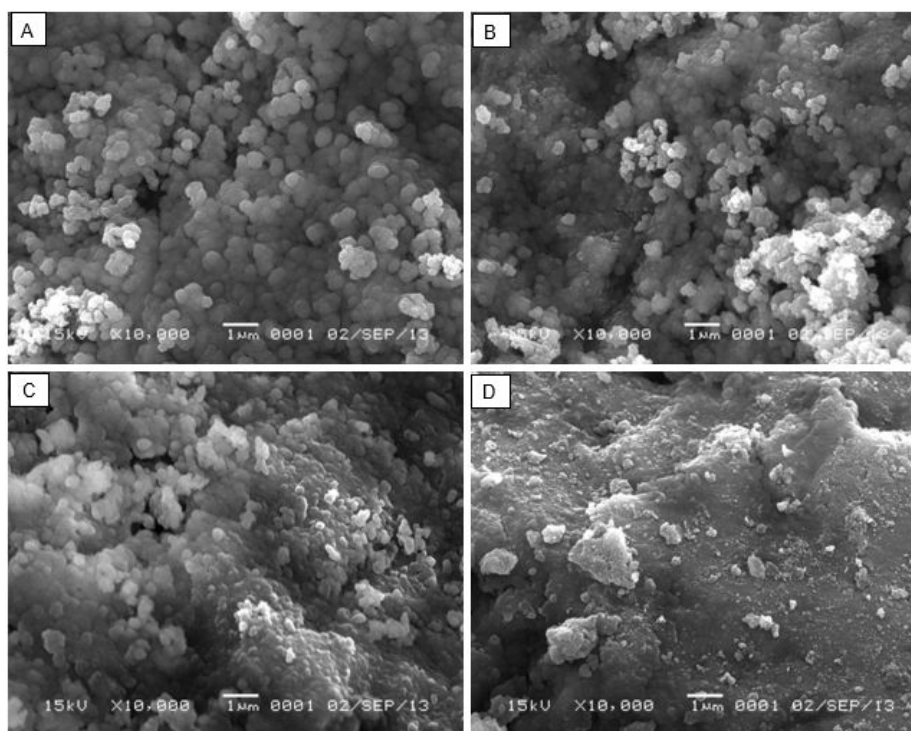


Fig 3. SEM image of (A) the MM, (B) UM, (C) MHT and (D) UMHT

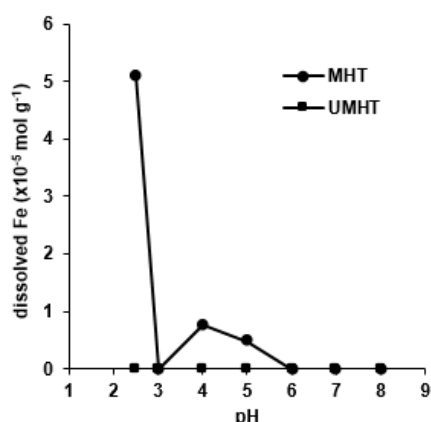


Fig 4. Stability curve magnetites in Mg/Al-NO₃ HT

resistance of Fe dissolved from Mg/Al-NO₃ hydrotalcite relatively high from pH 3 to 8, but at pH 2.5 magnetite was not stable (Fig. 4). In this study, the influence of solution pH on the adsorption of [AuCl₄]⁻ was investigated in the pH range in which magnetite was stable. The adsorption of [AuCl₄]⁻ on both of MHT and UMHT tends to increase with the increasing of media acidity from pH 2.5 to 3 and then decrease rapidly from pH 3 to 8 (Fig. 5). The observed decrease at the [AuCl₄]⁻ adsorption at higher pH > 3 is attributed to the increase of competitive effect of OH⁻ anions in alkaline condition, while the decrease of the [AuCl₄]⁻ adsorption at lower

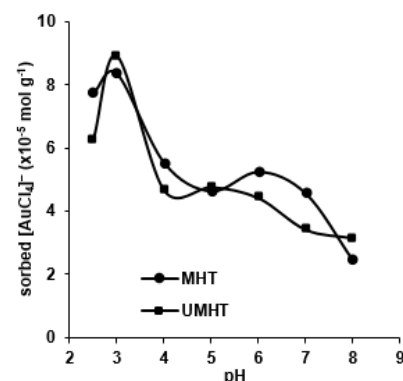


Fig 5. Effect of pH on the adsorption of [AuCl₄]⁻ on MHT and UMHT (initial [AuCl₄]⁻ concentration 25 mg L⁻¹; solution volume 10 mL; adsorbent dose 0.01 g)

pH < 3 is attributed to the MHT or UMHT materials may be partly dissolved. At pH < 3 or high media acidity, the hydroxide groups in the MHT or UMHT are protonated, their bonds to Mg and Al or both of them are broken and, therefore, occur the dissolution of metal cations [22]. A maximum [AuCl₄]⁻ adsorption is achieved at pH 3.

Effect of Contact Time on [AuCl₄]⁻ Adsorption

Fig. 6 shows the variation of the adsorption of [AuCl₄]⁻ during the adsorption process at various

contact times. It is seen that the $[\text{AuCl}_4]^-$ adsorption is increased greatly as the contact time is increased from 0 to 60 min, and then tends to be constant when the contact time is longer than 60 min indicating an equilibrium state. Hence, the equilibrium time of 60 min was applied for study of adsorption isotherms of both MHT and UMHT. Fig. 6 demonstrates that the adsorption capacity of $[\text{AuCl}_4]^-$ on MHT is larger than UMHT.

Adsorption Kinetics

Lagergren's pseudo first-order, Ho's pseudo second-order and second-order and Santosa's first order models were used to analyze the sorption kinetics. The Lagergren's equation for pseudo first-order kinetics can be written as follows [23]:

$$\ln(q_e - q_t) = \ln q_e - k_1 t \quad (1)$$

where q_e is the amount of adsorbate adsorbed (mol/g) at equilibrium and q_t is the amount of adsorbate adsorbed (mol g^{-1}) at time t , k_1 is the pseudo first-order rate constant (min^{-1}). Pseudo first-order kinetic plotted at 25 °C is given in Fig. 7a. The Lagergren's first-order rate constant (k_1) and theoretical equilibrium adsorption capacity (q_e) were calculated from the intercept and slope of the plot $\ln(q_e - q_t)$ versus t .

Pseudo second-order model is represented as [24]:

$$\frac{t}{q_t} = \frac{1}{k_2 q_e^2} + \frac{1}{q_e} t \quad (2)$$

where q_e and q_t have the same meaning as mentioned previously and k_2 is the rate constant for the pseudo second-order kinetics. The plots of t/q_t versus t are shown in Fig. 7b and the k_2 and q_e calculated from the

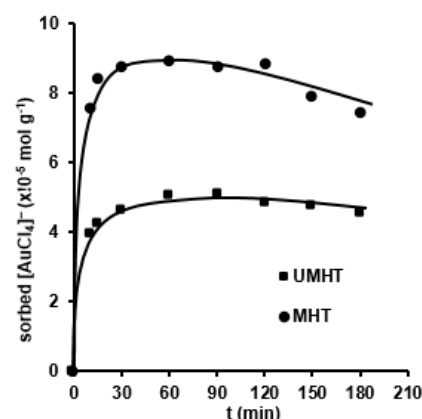


Fig 6. Effect contact time on the adsorption $[\text{AuCl}_4]^-$ with MHT and UMHT (initial $[\text{AuCl}_4]^-$ concentration 25 mg L^{-1} ; solution volume 10 mL; adsorbent dose 0.01 g)

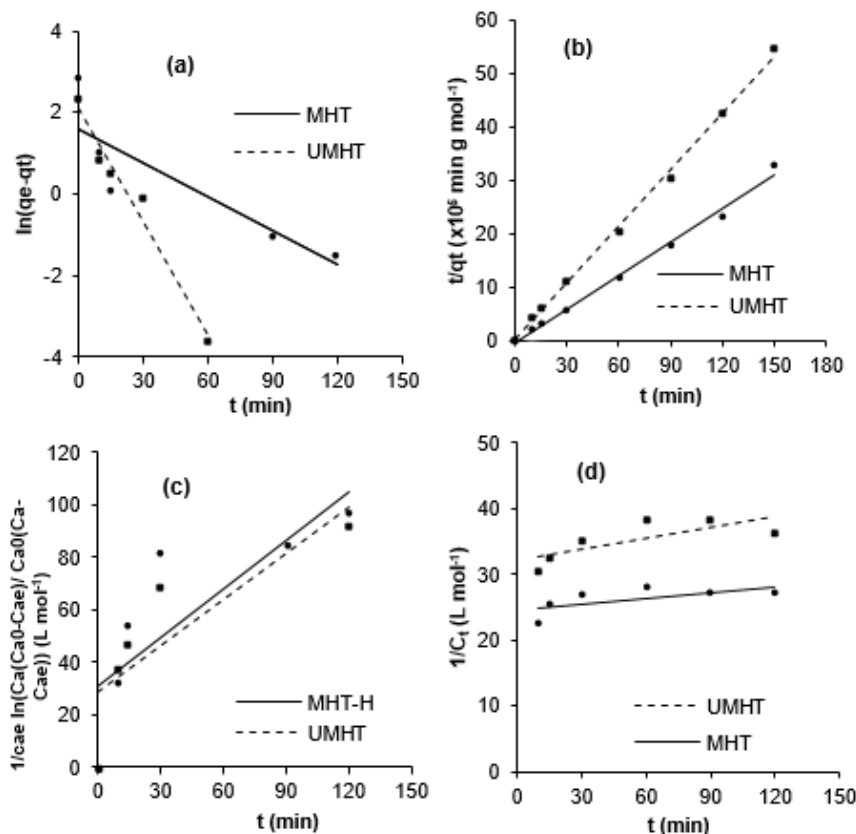


Fig 7. Plot of kinetics model for (a) pseudo first-order, (b) pseudo second-order, (c) first order and (d) second order

Table 1. Kinetic parameters of the pseudo first-order, pseudo second-order, first-order and second-order model for adsorption $[\text{AuCl}_4]^-$ on both of MHT and UMHT

Model	Parameter	MHT	UMHT
Lagergren's pseudo first-order	R^2	0.757	0.971
$\ln(q_e - q_t) = \ln q_e - k_1 t$	q_e (mol g ⁻¹)	1.47×10^{-5}	2.42×10^{-5}
	k_1 (min ⁻¹)	0.028	0.093
	Ho's pseudo second-order	R^2	0.999
$\frac{t}{q_t} = \frac{1}{k_2 q_e^2} + \frac{1}{q_e} t$	q_e (mol g ⁻¹)	5.16×10^{-5}	2.83×10^{-5}
	k_2 (g mol ⁻¹ min ⁻¹)	2.87×10^4	7.37×10^4
Santosa's first-order	R^2	0.666	0.694
$\frac{1}{C_{ae}} \ln \left(\frac{C_a (C_{a0} - C_{ae})}{C_{a0} (C_a - C_{ae})} \right) = k_s t$	k_s (L mol ⁻¹ min ⁻¹)	0.615	0.592
	Ho's second-order	R^2	0.442
$\frac{1}{C_t} = k_2 t + \frac{1}{C_0}$	k_2 (g mol ⁻¹ min ⁻¹)	0.029	0.055

Table 2. Parameter of Langmuir and Freundlich isotherm model for adsorption $[\text{AuCl}_4]^-$ on both MHT and UMHT

Model	Parameter	MHT-H	UMHT-H
Langmuir	R^2	0.965	0.949
$\frac{C_e}{q_e} = \frac{C_e}{q_m} + \frac{1}{K_L q_m}$	q_m (mg g ⁻¹)	31.250	66.667
	K_L (L mg ⁻¹)	0.120	0.066
	ΔG° (KJ mol ⁻¹)	26.662	25.169
Freundlich	R^2	0.898	0.947
$\ln q_e = \ln K_f + \frac{1}{n} \ln C_e$	K_f ((mg g ⁻¹) / (mg L ⁻¹) ⁿ)	2.842	2.353
	n	1.7	1.2

model. Second-order model is represented as [24]:

$$\frac{1}{C_t} = k_2 t + \frac{1}{C_0} \quad (3)$$

where C_t is the equilibrium concentration (mol L⁻¹), C_0 is the initial concentration (mol L⁻¹), t is the time (min), and k_2 is the rate constant (L mol⁻¹ min⁻¹).

The first order model is represented as [25]:

$$\frac{1}{C_{ae}} \ln \left(\frac{C_a (C_{a0} - C_{ae})}{C_{a0} (C_a - C_{ae})} \right) = k_s t \quad (4)$$

where C_{a0} is the initial concentrations of adsorbate (mol L⁻¹), C_a , and C_{ae} are the remaining concentrations of adsorbate in solution after adsorption at t and equilibrium (mol L⁻¹), respectively, k_s is the Santosa's first order rate constant, and t is the interaction time. The plots of

$\frac{1}{C_{ae}} \ln \left(\frac{C_a (C_{a0} - C_{ae})}{C_{a0} (C_a - C_{ae})} \right)$ versus t are shown in Fig. 7c. For

quantitative evaluation of the best kinetics model, correlation coefficients (R^2) were compared. The calculated kinetics parameters for $[\text{AuCl}_4]^-$ adsorbed on MHT and UMHT are shown in Table 1. The kinetic studies revealed that the pseudo-second order equation provided the best fit for the experimental data for all studied concentration values, confirming that the velocity control mechanism of adsorption is chemical adsorption [14].

Adsorption Isotherm

In the present investigation, the obtained results were analyzed following the isotherm models of Langmuir and Freundlich [26]. The Langmuir isotherm model is described by Eq. (5) and Freundlich isotherm model is described by Eq. (6):

$$\frac{C_e}{q_e} = \frac{C_e}{q_m} + \frac{1}{K_L q_m} \quad (5)$$

$$\ln q_e = \ln K_f + \frac{1}{n} \ln C_e \quad (6)$$

where q_e is the equilibrium adsorptive quantity of the adsorbate per gram of adsorbent (mg g⁻¹), C_e is the equilibrium adsorbate concentration (mg L⁻¹), q_m is the adsorption capacity (mg g⁻¹), n is the intensity of adsorption, K_L and K_f are Langmuir and Freundlich constants, respectively. The Langmuir model supposes that the adsorption surface possesses identical energetic sites and that each adsorbed molecule occupies a single site and the electrostatic connection consequently provides the formation of mono layered coverage of the adsorbate on the surface of the adsorbent. The Freundlich isotherm describes equilibrium on heterogeneous surfaces and for this reason, does not assume a capacity for adsorption in the monolayer [26]. From the value of K_L , the Gibbs's free energy will then calculated according to Eq. 7 [27]:

$$\Delta G^\circ = -RT \ln K_L \quad (7)$$

where, ΔG° is the Gibbs's free energy change, R is the universal gas constant, and T is the absolute temperature (K).

Fig. 8 shows the amount of adsorbed $[\text{AuCl}_4]^-$ on adsorptive surface versus the concentration of this anion in the equilibrium aqueous phase (effect of adsorbate concentration). The initial increase of the amount of adsorbed $[\text{AuCl}_4]^-$, with the increase of the modified adsorbate concentration, can be due to a highest availability of adsorption sites of adsorbents. However, for concentration value above 58.06 mol L^{-1} for MHT and $159.13 \text{ mol L}^{-1}$ for UMHT, with the increase of the adsorbate concentration, small changes occurred in the amount of adsorbed. This shows that adsorption ability of UMHT is much higher than that of MHT. The straight line equations obtained for the Langmuir model show larger correlation coefficients (R^2) than those of the Freundlich model for UMHT and MHT (Table 2), indicating the homogeneous nature of sample surface and formation of monolayer coverage of $[\text{AuCl}_4]^-$ on the surface of the adsorbent. In addition to R^2 , other calculated Langmuir and Freundlich parameters are reported in Table 2. From the q_m values given in Table 2, we know that every gram MHT and UMHT adsorbed $31.25 (9.19 \times 10^{-5} \text{ mol})$ the $66.67 \text{ mg} (1.96 \times 10^{-4} \text{ mol})$ $[\text{AuCl}_4]^-$, respectively. The energy of adsorption (ΔG°) was higher for MHT than UMHT. The hydrogen bonding between MHT/UMHT with $[\text{AuCl}_4]^-$ resulting ΔG° for MHT and UMHT in around -25 KJ mol^{-1} . The negative value of ΔG° indicates that adsorption process was spontaneous in nature. Thus the application of ultrasonic in preparation process generated many benefits in adsorption of $[\text{AuCl}_4]^-$ compared with the normal co-precipitation under mechanical stirring and shortened the

time required for preparation of crystalline Mg/Al- NO_3 hydroxalcalite-magnetite.

Desorption Study

Desorption experiment was carried out by NaOH solutions at a concentration ranging from 0.01 to 1 mol L^{-1} to regenerate the adsorbent. Trends of $[\text{AuCl}_4]^-$ desorption were increased initially with increasing concentration of NaOH and then reached a maximum on 0.5 mol L^{-1} NaOH for both MHT (25.32%) and UMHT (17.21%) (Fig. 9a). A higher percentage of $[\text{AuCl}_4]^-$ desorbed from MHT shows that $[\text{AuCl}_4]^-$ anion is weaker bound to MHT than UMHT. By applying 0.5 mol L^{-1} NaOH solution as eluent, the desorbed $[\text{AuCl}_4]^-$

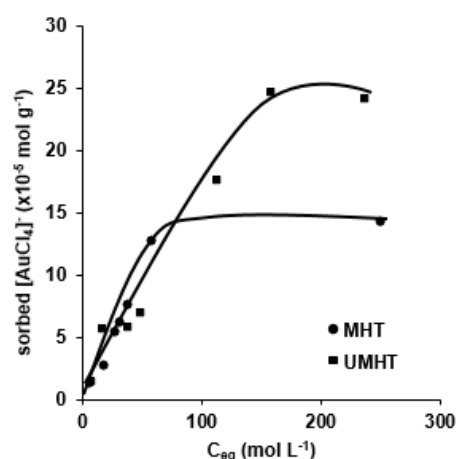


Fig 8. Effect of adsorbate concentration on the adsorption $[\text{AuCl}_4]^-$ with MHT and UMHT (adsorbent dose 0.01 g , initial $[\text{AuCl}_4]^-$ concentration 25 mg L^{-1} ; solution volume 10 mL ; temperature 25°C)

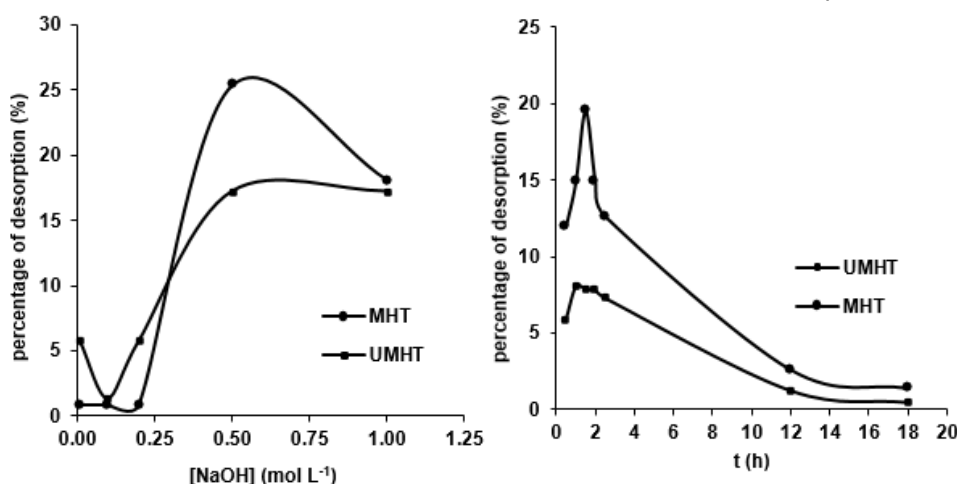


Fig 9. Effect of the concentration of NaOH solution (a) and desorption time (b) on the desorption of $[\text{AuCl}_4]^-$ (adsorbent dose 0.01 g , solution volume 10 mL , initial concentration of $[\text{AuCl}_4]^-$ 2.16 mg g^{-1} (MHT) and 1.36 mg g^{-1} (UMHT))

from MHT increased with increasing elution time to 1.5h and abruptly decreased above the elution time 1.5h. On the other hand, the maximum elution of $[\text{AuCl}_4]^-$ for UMHT was reached at elution time 1h (Fig. 9b).

CONCLUSION

Magnetite nanoparticles and Mg/Al- NO_3 HT-magnetite (MHT) as magnetic adsorbents were successfully prepared through co-precipitation method with the involvement of ultrasonic radiation, the preparation time for the prepared material (UMHT) became much shorter. Adsorption of $[\text{AuCl}_4]^-$ on MHT and UMHT was affected by pH and contact time. It was found that the optimum pH was 3 and by the employment of 10 mL of 7.35×10^{-5} mol/L $[\text{AuCl}_4]^-$ solution and 0.01 g adsorbent, the adsorption equilibrium was reached at contact time 60 min for both of MHT and UMHT. The kinetics of adsorption of $[\text{AuCl}_4]^-$ on both MHT and UMHT was well described by the pseudo second-order kinetic. The adsorption capacity of $[\text{AuCl}_4]^-$ on UMHT was higher than MHT, while percentage desorption of $[\text{AuCl}_4]^-$ on UMHT was lower than MHT. In addition to speed up preparation time, ultrasonic radiation technique can reduce the size of the adsorbent thereby increasing the adsorption capacity of the adsorbent to $[\text{AuCl}_4]^-$ in the aqueous solution.

ACKNOWLEDGEMENT

The authors would like to thank Directorate General of Higher Education (DGHE), Ministry of National Education Republic Indonesia for providing the financial support through doctoral dissertation research grant, contract number DIPA-023.04.1.673453/2015.

REFERENCES

- Parajuli, D., Adhikari, C.R., Kawakita, H., Yamada, S., and Ohto, K., 2009, *Bioresour. Technol.*, 100 (2), 1000–1002.
- Li, J., Lu, H., Guo, J., Xu, Z., and Zhou, Y., 2007, *Environ. Sci. Technol.*, 41 (6), 1995–2000.
- Changmei, S., Guanghua, Z., Chunhua, W., Rongjun, Q., Ying, Z., and Quanyun, G., 2011, *Chem. Eng. J.*, 172 (2-3), 713–720.
- Zhao, Y.Z., 2006, *Gold*, 27, 42–44.
- Gomes, C.P., Almeida, M.F., and Lourerio, J.M., 2001, *Sep. Purif. Technol.*, 24 (1-2), 35–57.
- Zhang, H., Jeffery, C.A., and Jeffrey, M.I., 2012, *Hydrometallurgy*, 125-126, 69–75.
- Akita, S., Yang, L., and Takeuchi, H., 1996, *Hydrometallurgy*, 43 (1-3), 37–46.
- Ranjbar, R., Naderi, M., Omidvar, H., and Amoabediny, G., 2014, *Hydrometallurgy*, 143, 54–59.
- Rabiega, M.P., and Trochimczuk, A.W., 2014, *Hydrometallurgy*, 146, 111–118.
- Chen, D., Li, Y., Zhang, J., Zhou, J., Guo, Y., and Liu, H., 2012, *Chem. Eng. J.*, 185-186, 120–126.
- Li, S.K., Huang, F.Z., Wang, Y., Shen, Y.H., Qiu, L.G., Xie, A.J., and Xu, S.J., 2011, *J. Mater. Chem.*, 21, 7459–7466.
- Shen, Y.F., Tang, J., Nie, Z.H., Wang, Y.D., Ren, Y., and Zuo, L., 2009, *Sep. Purif. Technol.*, 68 (3), 312–319.
- Chen, C., Gunawan, P., and Xu, R., 2011, *J. Mater. Chem.*, 21, 1218–1225.
- Chen, D., Li, Y., Zhang, J., Li, W., Zhou, J., Shao, L., and Qian, G., 2012, *J. Hazard. Mater.*, 243, 152–160.
- Petcharoen, K., and Sirivat, A., 2012, *Mater. Sci. Eng., B*, 177 (5), 421–427.
- Meng, J.H., Yang, G.Q., Yan, L.M., and Wang, X.Y., 2005, *Dyes Pigm.*, 66 (2), 109–113.
- Lu, W., Shen, Y., Xie, A., and Zhang, W., 2010, *J. Magn. Magn. Mater.*, 322 (13), 1828–1833.
- Olanrewaju, J., Newalkar, B.L., Mancino, C., and Komarneni, S., 2000, *Mater. Lett.*, 45 (6), 307–310.
- Frost, R.L., Spratt, H.J., and Palmer, S.J., 2009, *Spectrochim. Acta, Part A*, 72 (5), 984–988.
- Xiao, L., Ma, W., Han, M., and Cheng, Z., 2010, *J. Hazard. Mater.*, 186 (1), 690–698.
- Chang, Q., Zhu, L., Luo, Z., Lei, M., Zhang, S., and Tang, H., 2011, *Ultrason. Sonochem.*, 18 (2), 553–561.
- Herald, E., Triyono, Wijaya, K., and Santosa, S.J., 2011, *Indones. J. Chem.*, 11 (2), 117–123.
- Chai, P., Zheng, H., Wang, C., Ma, H., Hu, J., Pu, Y., and Liang, P., 2012, *J. Hazard. Mater.*, 213-214, 100–108.
- Ho, Y.S., and McKay, G., 1999, *Process Biochem.*, 34 (5), 451–465.
- Santosa, S.J., 2014, *CLEAN-Soil Air Water*, 42, 760–766.
- dos Santos, R.M.M., Goncalves, R.G.L., Constantino, V.R.L., da Costa, L.M., da Silva, L.H.M., Tronto, J., and Pinto, F.G., 2013, *Appl. Clay Sci.*, 80-81, 189–195.
- Jaiswal, A., Mani, R., Banerjee, S., Gautam, R.K., and Chattopadhyaya, M.C., 2015, *J. Mol. Liq.*, 202, 52–61.